Accommodation processes during deformation of nanocrystalline palladium

D.V. Bachurin [a], P. Gumbsch [a,b]

October 26, 2012

[a] *Institut für Zuverlässigkeit von Bauteilen und Systemen (IZBS), Karlsruher Institut für Technologie, 76131 Karlsruhe, Germany*
[b] *Fraunhofer Institut für Werkstoffmechanik (IWM), 79108 Freiburg, Germany*

Abstract

Atomistic simulations of uniaxial tensile and compressive straining of three-dimensional nanocrystalline palladium were performed at room temperature and different strain rates. Detailed analysis revealed that initial plastic deformation is due to grain boundary sliding accommodated by localized bending inside the grains and the formation of dislocation embryos. Intergranular cracking in the absence of dislocation activity was found at later stages of tensile straining. During compressive straining the sample shows a plastic response which is brought about mainly by intergranular accommodation processes. The contribution of extended partial dislocations emitted from the grain boundaries as well as full dislocations and twinning at later stages of deformation to the total strain was found to be insignificant.

Keywords: Nanocrystalline materials; Mechanical properties; Dislocation; Grain boundaries; Molecular dynamics

1 Introduction

High yield stresses and strain-rate sensitivity but limited tensile elongation before fracturing [1–3] are characteristic features of nanocrystalline metals. Their properties are mostly explained by the peculiarities of the microstructure: small grain sizes, the large number of grain boundaries and the presence of porosity relating to synthesis. Of course, the limited ductility is a major concern and the target of many investigations.

Experimentally nonintrusive investigation of nanocrystalline materials during deformation is not possible but parallel computing platforms today allow to atomistically simulate three-dimensional nanocrystalline structures with grain sizes of the same order as can be achieved experimentally [4–12]. These techniques are then often applied to analyse the processes occurring during deformation – although only on very small time scales of nanoseconds.

Plastic deformation of coarse-grained materials is mainly carried by dislocations within the individual grains. It is believed that dislocations are generated by sources inside the grain. Decreasing the grain size down to the nanometer scale prohibits conventional operation of dislocation sources. Numerous computer simulations have revealed the following main deformation mechanisms of three-dimensional nanocrystalline fcc metals:

- Dislocations are emitted from the grain boundaries, travel through the grain and absorb in the opposite grain boundaries without leaving dislocation debris (e.g. [5, 7, 8]).
- Dislocations are nucleated at ledge structures in the grain boundaries. These ledges are concentrators of shear and hydrostatic stresses arising because of sliding incompatibility between the grains (e.g. [6, 12]).
- Nucleation and propagation of the dislocation are two separate processes. Dislocation embryos are often nucleated, but do not propagate. Propagation needs an unpinning, which is strongly temperature dependent (e.g. [11, 12]).
- The type of observed dislocation activity (extended partials or full dislocations) can be understood in terms of the generalized planar fault energy curve for an intrinsic stacking fault (e.g. [9]).
- For very small grain sizes ($d < 10\ nm$), plasticity is believed to be carried mostly by grain boundary accommodation mechanisms (e.g. [4, 7, 8, 10]).

The investigations reported here are part of a combined experimental and simulation effort to better understand the deformability of nanocrystalline fcc metals

and alloys. Palladium is chosen as the model material since it is accessible both experimentally and by simulations and it can be alloyed in a controlled manner. Also its stacking fault energy is reasonably high so that the operation of full dislocations can be expected.

There are only a few previous computer simulation studies of the deformation behavior of fully three-dimensional nanocrystalline palladium structures (e.g. [8]). The interatomic potential used in these studies [8] gives an unrealistically low stacking fault energy of 0.008 J/m^2 compared to the experimental value of 0.180 J/m^2 [13]. This is believed to markedly influence the deformation behavior. The purpose of the present paper is to atomistically simulate the mechanical response of nanocrystalline palladium at room temperature in uniaxial deformation at different strain rates using an improved interatomic potential which gives reasonable dislocation properties.

The paper is organized as follows: in Section 2 the simulation methods and sample preparation are described; the results of the tensile and compressive straining and detailed investigation of the atomic configurations and of the observed deformation mechanisms are presented in Section 3 and 4; the results are discussed in Section 5.

2 Simulation methods and sample preparation

Molecular dynamics simulations were performed using the molecular dynamics code IMD [14]. Static relaxation was performed using the FIRE algorithm [15]. An Embedded Atom Method potential for palladium [16] is used, which is fitted to density functional calculations and the intrinsic stacking fault energy [17]. This potential was selected since it reproduces unstable and stable stacking fault energies well and is therefore expected to realistically describe the structure of full and partial dislocations. However, the potential gives an unrealistically low surface energy which will lead to premature fracture. This is not *per se* regarded as harmful for the investigation of plastic deformation but limits the applicability of the potential under tensile conditions.

The initial three-dimensional nanocrystalline structures [18] were generated using the Voronoi construction and provided to us by the group at the Paul Scherrer Institute. The sample contains 100 defect-free and randomly oriented grains with a mean grain size of 10 nm and approximately 4.6 million atoms (see Fig. 1). Grain size and grain boundary misorientation distributions of the specimen are shown in Fig. 2. The deformation behavior of exactly this nanocrystalline structure has been investigated earlier for aluminum [18]. The adaption of the sample for the present investigations consisted of the following steps. Initially the sample was rescaled from aluminum to palladium equilibrium lattice constant. After static relaxation it was

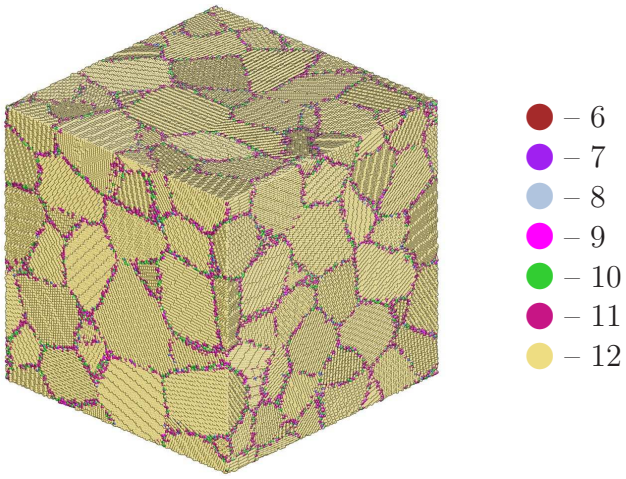

Figure 1: Computer-simulated sample of nanocrystalline palladium with a mean grain size of 10 nm. Each side of the box is approximately 41 nm long. Atoms are colored according to their coordination number. Yellow atoms correspond to the ideal fcc crystal lattice, other colored atoms are grain boundary atoms.

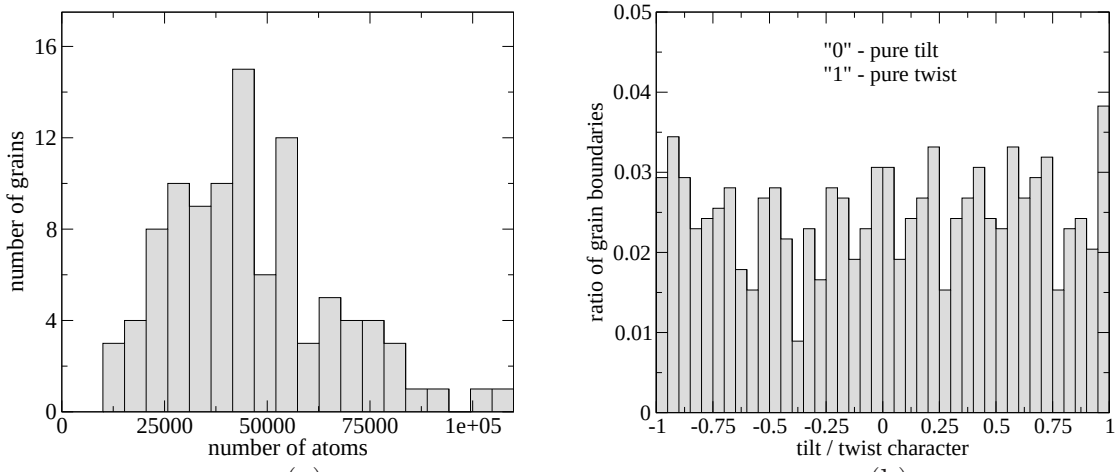

(a) (b)

Figure 2: Grain size (a) and grain boundary misorientations (b) distributions of the nanocrystalline palladium sample shown in Fig. 1.

annealed for 10 ps at 1360 K (85% of the melting temperature of the potential) and then equilibrated for 20 ps at 300 K. The density of the undeformed sample at 300 K is 96.6% of the perfect crystal value. The percentage of defect atoms (atoms with coordination numbers unequal to 12 calculated with a cutoff radius of 3.38Å) is 13.1%.

Uni-axial strain with strain rates of $10^7 - 10^9\ s^{-1}$ was applied by continuously

scaling the atomic coordinates and box-sizes along the x direction. Along the two other directions, the stresses were kept equal to zero, so the system could change its size freely. The strain rate of 10^7 s^{-1} is the lowest strain rate at which a reasonable plastic deformation could be achieved in an acceptable computer time with the available computational resources. Molecular dynamics simulations were performed at a constant temperature of 300 K with periodic boundary conditions in all directions.

In order to identify twin planes and stacking faults in the grains, the Honeycutt and Andersen analysis was applied, which allows to classify pairs of atoms according to their local environment [19]. Using this technique three different classes of atoms were defined: fcc atoms (green), first neighbor hcp coordinated atoms (red); other atoms (blue). The atomic structures were visualized with the program AtomEye [20].

3 Tensile straining

Figure 3a displays the global stress-strain curves for the application of uniaxial tensile strain. The curves in Fig. 3a clearly show a strong strain rate sensitivity of the nanocrystalline palladium. Larger strain rates lead to higher stresses. The curves reach their maxima at different strains. Larger strain rates give larger strains at which the stress-strain curve has a maximum. The stress-strain curves clearly begin to deviate from the linear slope at a strain of about 0.7%. As a criterion we used 0.005% of plastic strain to define a deviation of the stress-strain curve from the linear slope.

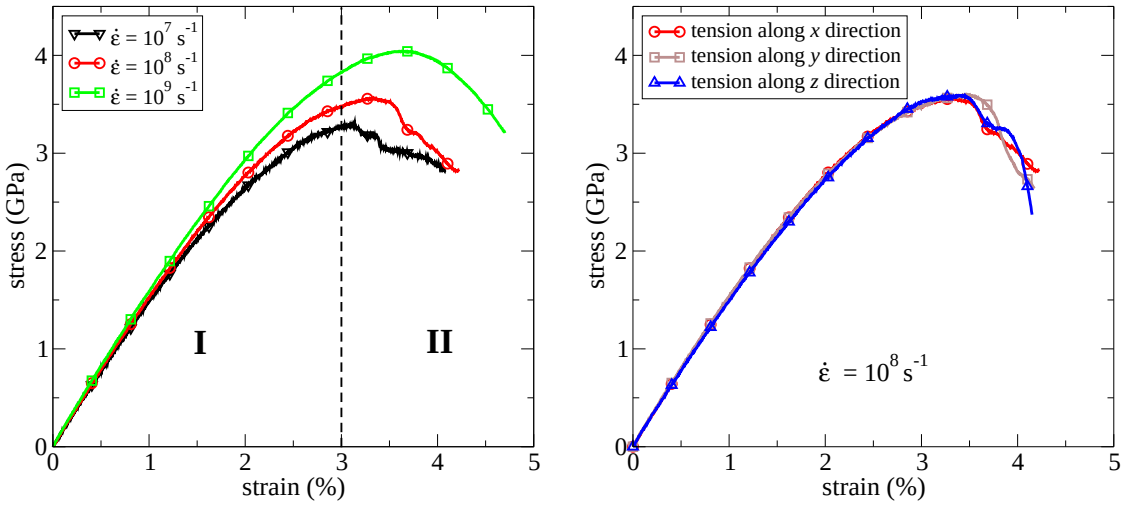

Figure 3: Stress-strain curves for nanocrystalline palladium at an applied uniaxial tensile strain: (a) with three different strain rates and (b) with three different directions of the applied strain in the given microstructure.

Figure 3b shows the results of the application of the uniaxial tension along x, y and z directions of the specimen in Fig. 1. All three curves are very similar and, as expected, there are no significant differences for these three different uniaxial straining directions of the specimen. This confirms the absence of any anisotropy or crystallographic texture in the sample.

The stress-strain curves in Fig. 3a can be approximately divided into two regions: I (0–3% strain) and II ($>$ 3% strain). In the following, the atomic configurations and deformation mechanisms in these two regions will be analysed.

3.1 *Region I (0–3% tensile strain)*

The deviation of the stress-strain curve (with the strain rate of 10^8 s^{-1}) from the linear slope in palladium begins at a strain of 0.7%. This is approximately two times higher than reported for aluminum [21] and suggests that the relevant accommodation processes in nanocrystalline aluminum start to operate earlier and faster than in nanocrystalline palladium.

The elastic regime is followed by a small plastic regime. No extended partial or full dislocations were found up to a strain of 3%. However, several dislocation embryos are found near grain boundaries. The maximum number of dislocation embryos observed in one grain was five. These embryos do not necessary belong to the same glide system. Three possible types of embryo behavior were recorded: (1) several embryos were generated after some deformation; (2) other dislocation embryos already exist in the initial structure as a result of the relaxation of the grain boundary structure. They then either stayed near the grain boundary without any visible change or were partially emitted into the grain; (3) some dislocation embryos that existed in the initial configuration entered back into the grain boundary during deformation. Sites of embryo nucleation could generally be correlated with hydrostatic stress concentrations at the grain boundaries before nucleation.

Figure 4(a-c) show cross-sections of different grains along (111) planes at 3% strain. Embryonic dislocations are clearly seen in the grain boundaries (Fig. 4a,b). They did not propagate into the grains. Figure 4c displays the only case of nucleation of a full dislocation observed in all simulations. The nucleation of the full dislocation started by the emission of a leading partial dislocation. The trailing partial dislocation was thereafter emitted from a nearby position at the grain boundary. The dislocation, however, remained in the position shown in Figure 4c and did not propagate through the grain during the course of the entire simulation. This full dislocation is jogged. Segments of the dislocation line extend over more than one plane as shown in Fig. 4d. The Schmid factor for the active slip system is 0.45 and the resolved shear stress calculated from the applied strain is 1.55 GPa. It is

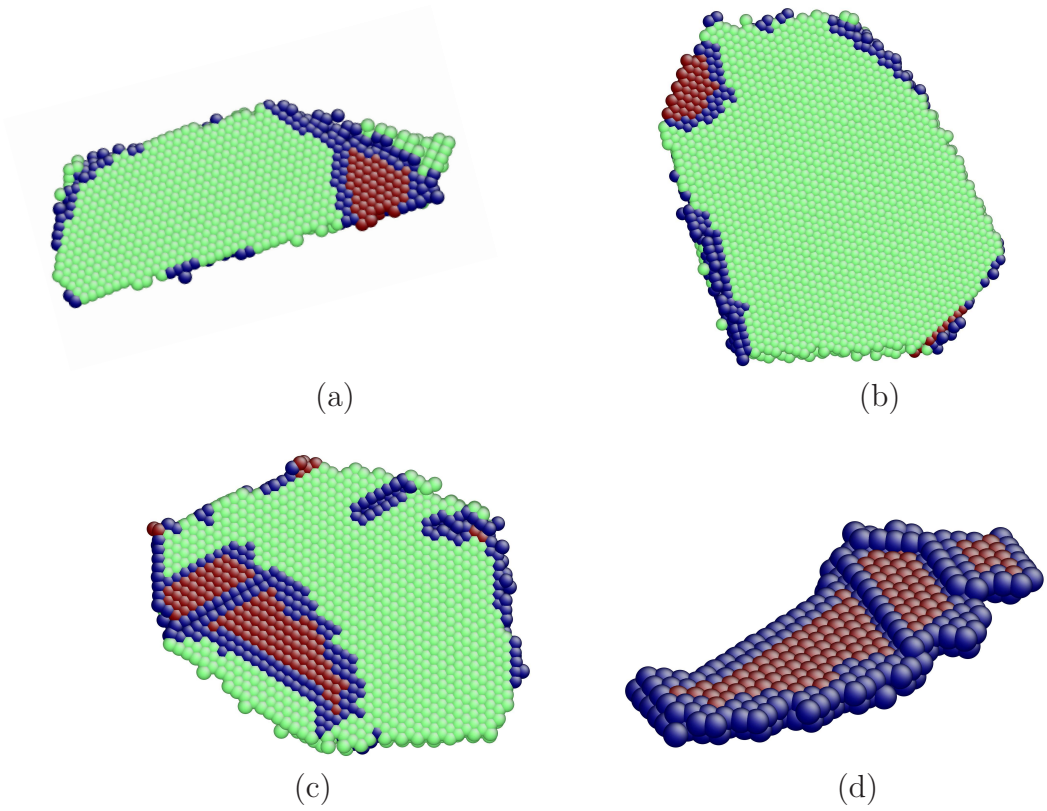

Figure 4: Dislocation activity in different grains at tensile strain of 3%. Partial dislocation embryos in the grain 11 (a) and grain 79 (b); partial propagation of the full dislocation embryo into the grain 8 (c). The full dislocation (c) is jogged (d). Atoms are colored according to their local crystalline structure.

worth noting that the active glide system in this grain is not the one which experiences maximum resolved shear stress. Furthermore, there are other grains with pre-existing dislocation embryos and higher resolved shear stress, where the embryos do not propagate. This must be due to pinning sites for those embryos at the grain boundaries. For comparison, Fig. 4b shows the leading partial dislocation embryo in grain 79. Even at 3% strain the dislocation can not be emitted although it is almost ideally oriented and experiences large resolved shear stress which can also be seen from the small radius of curvature of this partial dislocation.

The general absence of dislocation activity in the grains but clear deviation from elastic behavior in the stress-strain curve indicates that intergranular processes must be active. Indeed, detailed inspection of the atomic configurations shows displacements of the grain boundary atoms. This suggests that grain boundary accommodation processes may play an important role.

Figure 5 illustrates that accommodation processes do not involve significant grain boundary migration. Three mutually perpendicular cross-sections of the sample are

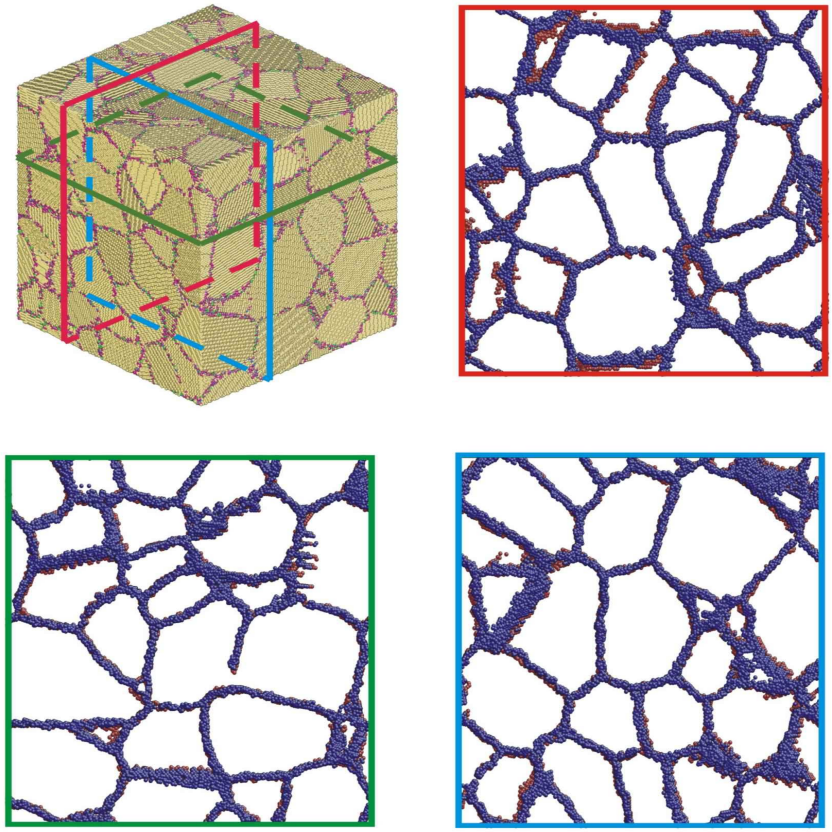

Figure 5: Illustration of the grain boundary migration in nanocrystalline palladium. Three mutually perpendicular cross-sections of the sample are shown with different colors: red (normal x), green (normal y), blue (normal z). Blue colored atoms belong to the cross-section of the undeformed sample, red atoms belong to the same cross-section, but made in the sample after 3% of tensile strain. Only non-12-fold coordinated atoms were made visible.

shown. Two nanocrystalline structures – undeformed (blue-colored atoms) and after tensile deformation of 3% strain (red-colored atoms) – were superposed in every cross-section. In this figure the 12-coordinated atoms are omitted for clarification. Very small amounts of grain boundary migration can be recognized on some of the grain boundaries in Fig. 5. However, overall there is only very little migration on all cross-sections. No significant straightening and migration of triple junctions was observed either up to 3% tensile strain.

Numerous events of grain boundary sliding were found in nanocrystalline palladium. Figure 6a,b displays atomic rearrangements near grain boundaries and triple junctions. The thickness of the displayed cross-sections of the grains in Fig. 6 is 5Å. The atoms are shown as black circles at their position prior to straining. Relative atomic displacements are visualised by the displacement vectors which indicate

the difference between the position of the atoms prior to tensile deformation and at 3% strain. The arrow of the vector indicates the position of the same atom after straining. Displacements are not magnified. The atomic rearrangements are different from the grain boundary sliding that has been reported earlier in nanocrystalline nickel [22] in the fact that the sliding reported here is associated with highly inhomogeneous elastic displacements in the grains. The grains sometimes slide as a whole along only one of the grain boundaries. Sliding is localized and accommodated by elastic strain and bending of parts of the grain.

Figure 6a shows grain boundary sliding between the 'large' central and the two upper grains. It is clearly seen, that the central grain does not slide as a whole block by means of rigid-body translation. The atoms near the upper grain boundaries exhibit elastic displacements slightly inclined in the direction of applied strain, and the values of the relative atomic displacements decreases to the center of the grain. Atomic activity near another triple junction is demonstrated in Fig. 6b. Only the atoms in the corner of the upper left grain are elastically distorted; the displacements of the atoms in the other two grains near this triple junction are small. The local environment analysis for the structures in Fig. 6a,b does not show the presence of any dislocation embryos near the grain boundaries and triple junctions, where elastic displacements of the atoms were observed. Grain rotation was not observed in our molecular dynamics simulations.

Small embryos of cracks nucleate at the grain boundaries at about 3% strain. However, these precursors to cracks are shorter than the grain boundary segment on which they are nucleated and do not propagate into the adjacent grain boundaries.

3.2 *Region II (> 3% tensile strain)*

The stress-strain curves in Fig. 3a reach maxima and then begin to rapidly decrease for all strain rates. Numerous dislocation embryos in the grain boundaries and no extended partials or full dislocations were found when the curves reach their maxima. The absence of any dislocation activity was confirmed by slip vector analysis. Thereafter intergranular cracking starts irrespective of strain rate. The cracks first nucleate at the grain boundaries which are oriented perpendicular to the direction of applied strain and then propagate along other adjacent grain boundaries as shown in Fig. 7. Intergranular cracking initiates at high-angle grain boundaries of mixed character (tilt and twist) with misorientation angles between 26° and 45° and occurs at the same locations independently on the strain rate. The analysis reveals no difference between tilt and twist boundaries. Both show intergranular cracking. However, there are high-angle grain boundaries oriented perpendicular to the direction of straining that do not crack.

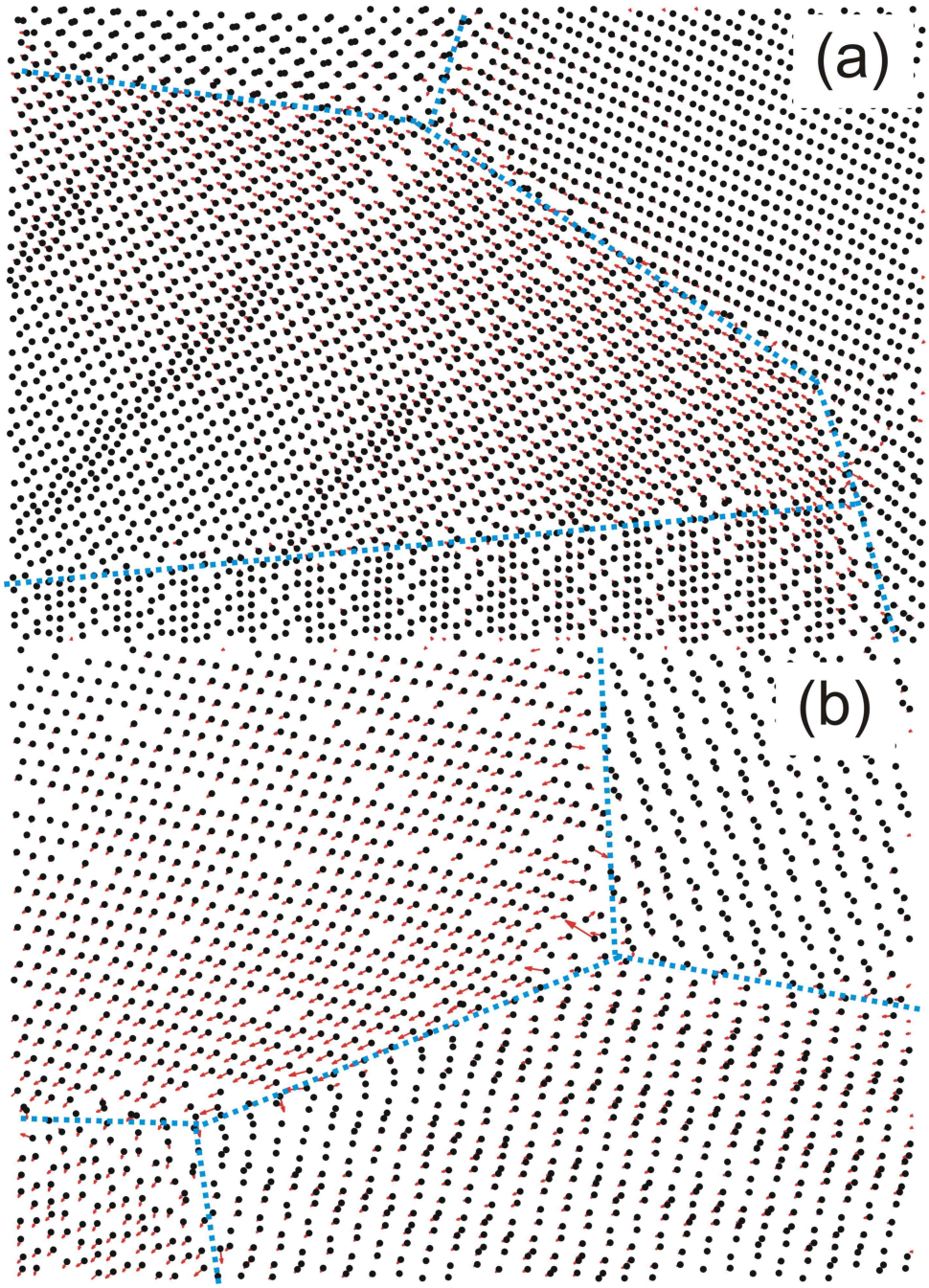

Figure 6: Illustration of the grain boundary accommodation processes in nanocrystalline palladium: (a) grain boundary sliding; (b) atomic activity near the triple junction. The blue dash lines in the figure shows the position of the grain boundary planes.

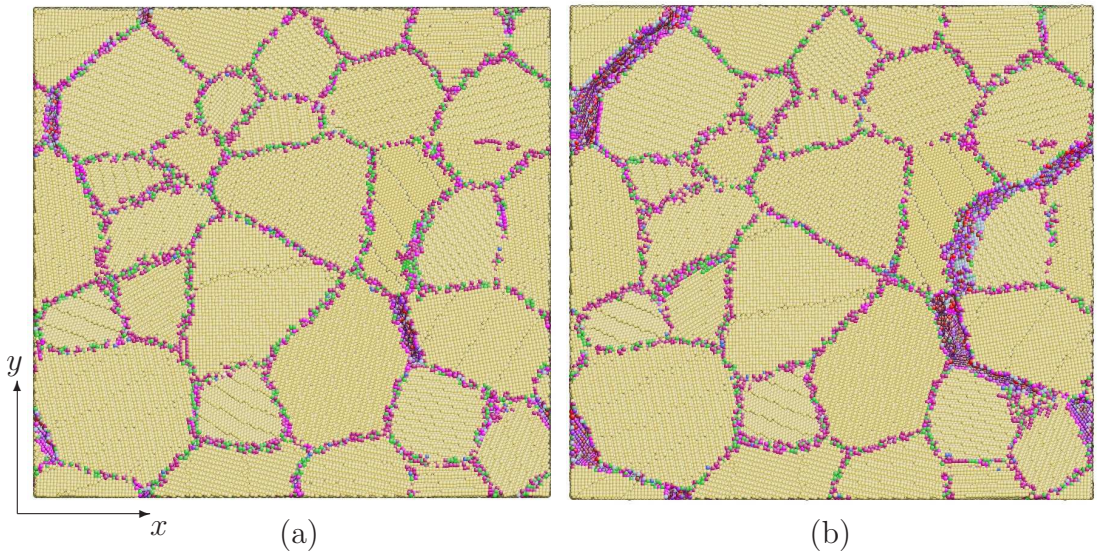

Figure 7: xy cross-sections of the sample. Different stages are displayed: (a) at 4% strain and (b) the evolution at 5% tensile strain. The cross-sectional view (a) clearly shows that the cracks open along grain boundaries, which are oriented perpendicular to applied strain, and then propagate along adjacent grain boundaries (b). Atoms are colored according to their coordination number.

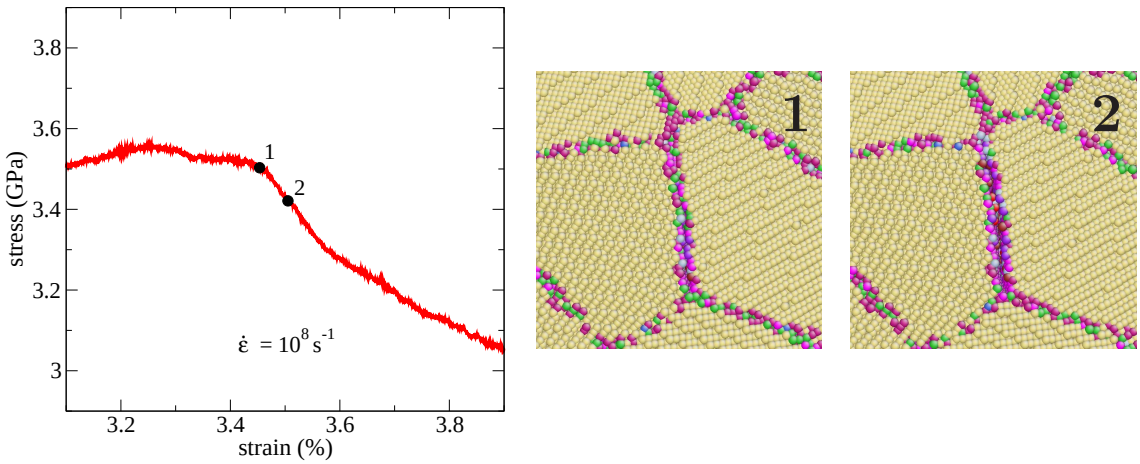

Figure 8: A part of the stress-strain curve for applied uniaxial tensile strain (left) and the fragments of the nanocrystalline structures at 3.45% and 3.51% strain (right). Crack formation begins at the triple junction and then continues at the grain boundary, the plane of which is perpendicular to the direction of applied strain. The drop of the curve corresponds to the opening of the crack in the grain boundary. Atoms of the nanocrystalline structures are colored according to their coordination number.

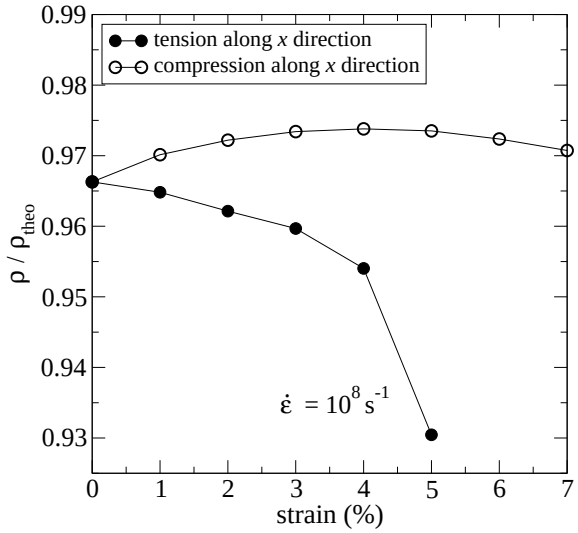

Figure 9: The dependences of the relative density of the nanocrystalline palladium sample versus applied uniaxial tensile and compressive strains.

The part of the stress-strain response for tensile straining which is connected to the initiation of cracking is displayed on the left of Fig. 8. The fragment of the nanocrystalline structure at the points 1 (3.45% strain) and 2 (3.51% strain) are shown on the right of Fig. 8. The crack starts to open from one triple junction and then propagates along the grain boundary. The grain boundary plane is oriented almost perpendicular to the direction of applied strain. The drop of the stress-strain curve in Fig. 8 corresponds to the crack opening. No dislocation motion was associated with the cracking or the load.

The initiation of the cracking usually originates from triple junction. Figure 6 displays a precursor to such crack formation. The displacements of atoms in the large grain to the left, away from the triple junction, increase grain boundary free volume and will eventually lead to crack formation at higher applied strain.

Initiation of crack formation can be confirmed by inspection of the density change during the deformation process. Figure 9 shows the dependence of the relative density of the specimen on the applied uniaxial tensile strain. It is clearly seen, that the density of the sample linearly decreases with the applied strain in the elastic and in the early stage of the plastic regime up to 3% of tensile strain. At and above 4% the density drops more significantly indicating the beginning of fracture.

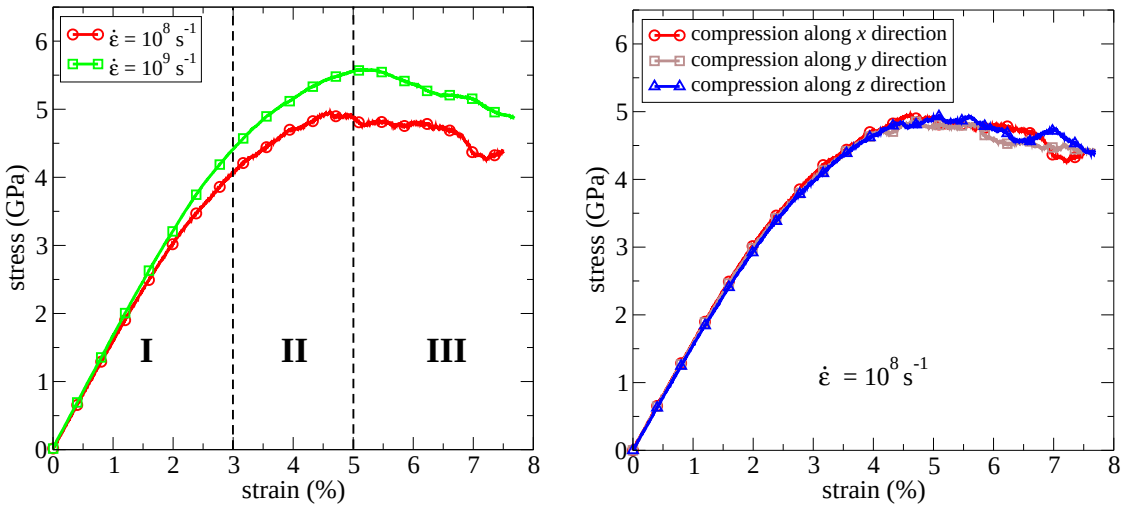

(a) (b)

Figure 10: Stress-strain curves for nanocrystalline palladium at an applied uniaxial compressive strain: (a) at two different strain rates and (b) with three different directions of an applied strain.

4 Compressive straining

Figure 10a shows the stress-strain curves for uniaxial compressive straining at two different strain rates of 10^8 and 10^9 s^{-1}. Similar to the tensile straining, the higher strain rate leads to a higher "flow stress". The stress-strain curves at different strain rates also reach their maxima at different strains. The curves begin to deviate from the linear slope at a strain of approximately 1.0%. This value is 1.4 times higher than for uniaxial tension. The application of uniaxial compression along x, y and z directions at a constant strain rate of 10^8 s^{-1} revealed again no significant differences of the mechanical behavior for the different directions (see Fig. 10b).

The stress-strain curves in Fig. 10 can be approximately divided into three regions: I (0–3% strain), II (3-5% strain) and III (> 5% strain). The atomic configurations and deformation mechanisms in every region are analysed separately.

4.1 *Region I (0-3% compressive strain)*

A small amount of plasticity is observed after the elastic regime (beyond 1.5% strain). No extended partial or full dislocations were found up to 3% strain. However, many embryos of partial dislocations were found near the grain boundaries. These embryos do not necessarily belong to the same glide system. The nucleation of the dislocations at compressive applied strain occurs at different grain boundaries and in different grains than in the tensile simulations. Almost half of the grains show no dislocation embryos at all. Investigation of grain boundary migration reveals that it

is small and of the same order as for tension. In general, the observed deformation mechanisms in this region are very similar to the ones for tensile straining.

4.2 *Region II (3-5% compressive strain)*

Detailed inspection of the atomic configurations shows that emission of partial dislocations occurs after 3% of compressive strain. The first fully extended partial dislocation was observed at a strain of 3.46%. At that strain, 88% of the maximum stress is reached. The number of extended partial dislocations is considerably increased with the increase of strain and, as it has been found previously for nanocrystalline aluminum [21], the total number of extended dislocations is approximately proportional to plastic strain. At 4% of total strain only four partial dislocations were observed in the grains No. 5 and 77. One of these extended partials is presented in Fig. 11a. It is interesting to note again that the slip event did not occur on the glide plane with the highest resolved shear stress.

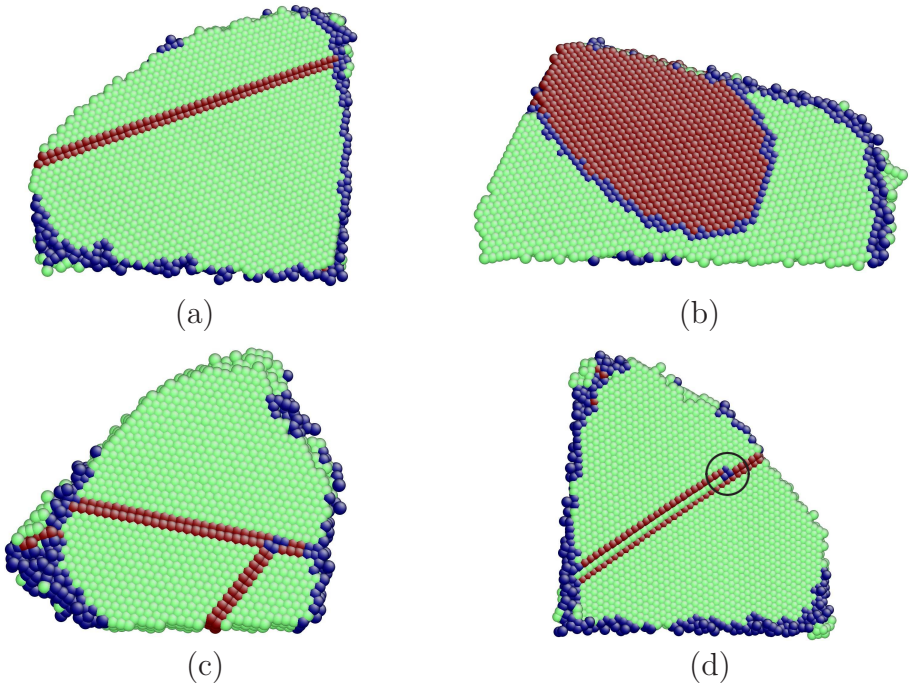

Figure 11: Partial dislocation activity in different grains during compressive straining: (a) extended partial dislocation at 4% strain; (b) traveling through the grain leading partial at 5% strain; (c) multislip at 5% strain; (d) micro-twinning process. The circle in figure (d) shows the trailing partial dislocation emitted on an adjacent slip plane to the initial partial, leaving a micro-twin behind. Atoms are colored according to their local crystalline structure.

Eleven extended partial dislocations, two cases of intersection of partials and

three cases of micro twinning were registered at 5% of total strain. Nucleation of dislocations mostly occurs near triple lines. Figure 11b displays a traveling partial nucleated near a triple junction. Before the leading partial dislocation in Fig. 11b reached the opposite grain boundary, an embryo of the trailing partial is nucleated (not presented in Fig. 11b) on an adjacent slip plane situated one interplanar spacing below. This is the first step of the formation of a microtwin. Figure 11c displays the cross-section of a grain which shows multiple slip events at 5% strain. The horizontal extended partial dislocation was emitted first. Thereafter the second partial was nucleated at the lower grain boundary. The Schmid factors for both glide planes in Fig. 11c are approximately the same. The traveling second partial dislocation meets the stacking fault left by the first partial and can not overcome this barrier at the current strain. This resembles a situation in submicrocrystalline materials, where the grain boundaries hinder dislocation activity, thereby forming dislocation pile-ups which lead to work hardening. Later stages of a twinning process are shown in Fig. 11d. The trailing partial dislocation (encircled) was emitted on an adjacent slip plane to the initial partial and leaves a micro-twin behind (one layer of green-colored fcc atoms between two layers of hcp atoms).

4.3 *Region III (> 5% compressive strain)*

In Region III at strains larger than 5% all types of dislocation activity – extended partial dislocations, twinning and full dislocations – were observed. After the emission of a first leading partial dislocation, nucleation of the trailing partial often occurs before the leading partial dislocation reached the opposite grain boundary. The nucleation of a trailing partial dislocation on the adjacent slip plane, i.e. twinning, was registered at lower strains ($\approx$ 5% strain) than the nucleation of the trailing partial on the same slip plane, i.e. emission of a full dislocations ($\approx$ 6% strain). Several cases of the growth of 3-layer deformation microtwins were observed.

Localized crack formation began at about 5% compressive strain at grain boundaries oriented approximately parallel to the direction of applied strain. These cracks were very small and remained localized within the grain boundaries. Analysis of atomic configurations has revealed that cracking occurs at the same grain boundaries irrespective to the strain rate. There is relation to the locations of the crack nuclei under tensile and compressive loading. Approximately in 50% cases crack opening is connected with the same triple junctions. Extensive intergranular fracture proceeded in Region III with the increase of strain. However, the cracks did not propagate along adjacent grain boundaries as it was the case for tensile straining. The length of the cracks did never exceed the length of the boundaries. Direct evidence that a crack is nucleated at the absorption site of a dislocation in a grain

boundary, which has been reported previously [23], was not found in our simulations.

The relative density during compressive straining increases up to 4% strain and then monotonously decreases (see Fig. 9). The value ρ/ρ_{theo} at 5% strain is little smaller than at 4% confirming an appearance of tiny cracks which were observed by direct visual inspection of nanocrystalline structures. Thereby, the density evolution during deformation seems to be a sensitive tool for detectivity fracture processes in compressive deformation.

5 Discussion

Only embryonic dislocations were observed in the grain boundaries below 3% of tensile or compressive strain. Nucleation of the embryos often occurs on slip planes that do not necessarily have the highest Schmid factor. This supports an approach suggested by Asaro and Suresh [24] in which embryonic dislocations are pictured as being emitted primarily from local stress concentrations at the grain boundaries. Our simulations reveals that embryonic dislocations do not immediately transmit into the grain. A critical shear stress must be reached to depin the embryo from the boundary. Propagation of the dislocation is associated with the overcoming of pinning points located within the grain boundaries. This seems to be a general feature of nanocrystalline fcc metals and was already noted previously [11].

Dislocation transmission through the grain boundaries into the neighboring grain, which was suggested as an important deformation mechanism in highly twinned materials [25–28], was not observed in the present investigations and only once in previous studies of realistic three-dimensional nanocrystalline materials [29]. It may therefore safely be assumed that direct transmission of dislocations from one grain to another does not play a significant role in the plastic deformation of nanocrystalline materials.

Dislocation activity in nanocrystalline palladium was observed only in compression. In the following, an estimate of the strain caused by dislocation slips is derived. Following [7] slipping of a dislocation with Burgers vector $\mathbf{b}$ through the system leads to a strain $\varepsilon_{xx} = b_x/h_x$, where b_x is the x component of the Burgers vector and h_x is the size of the simulation box in the x direction. If the dislocation passes through one grain and cover the area S, the contribution from this slip event to the ε_{xx} component of the strain can be calculated as:

$$\varepsilon_{xx} = \frac{b_x}{h_x} \cdot \frac{S\,cos\varphi}{h_y h_z} = \frac{b_x S\,cos\varphi}{V},$$

where $V = h_x h_y h_z$ is the volume of the simulation cell, φ is the angle between the slip plane and the yz plane. The projection of Burgers vector to the loading direction

is $b_x = b\,sin\varphi$, where $b = a_0/\sqrt{6}$ is the Burgers vector of Shockley partial and a_0 is the lattice constant. The total strain can be written as a sum of individual slip events

$$\varepsilon_{xx}^{total} = \frac{a_0}{2\sqrt{6}V} \sum_{i=1}^{n} S_i\, sin(2\varphi_i).$$

Summation over all extended partial dislocations and dislocation embryos (larger than 20 atoms) gives $\varepsilon_{xx}^{total} \approx 0.03\%$ at 4% of total compressive strain. For comparison, $\varepsilon_{xx}^{total} \approx 0.7\%$ at 7% of total compressive strain. Thus all observed dislocations (for details see 4.2) do not contribute significantly to the observed plastic strain. Therefore grain boundary sliding plays an important role and is the main deformation mechanism between 1% and 7% of total strain for both tensile and compressive deformation.

However, the grain boundary sliding, where a grain slides as a rigid block, is very rarely observed and was only found in the smallest grains. In most cases, only the atoms close to the grain boundaries and triple junctions are significantly displaced. Atoms in the center of the grain are more or less rigid (see Fig. 6). Such strongly inhomogeneous localized bending inside the grains of course depends on the structure of the grain boundaries at the triple junction. Some of the triple junctions can be "harder" than others and a bending near the grain boundary of only one grain takes place, as shown in Fig. 6b. In the case when all grain boundaries in the triple junction have approximately equal "hardness", the localized bending is shared between all three grains.

Obviously, this kind of elastic atomic displacement may contribute to the microstrain of pre-deformed nanocrystalline material. It is typically registered as potentially asymmetric peak broadening in X-ray diffraction. Investigating virtual diffractograms of undeformed samples with different grain sizes Stukowski et al. [30] have shown that the broadening of the Bragg reflections arises from long-range correlated displacement fields that extend throughout the grains. We suppose that deformation leads to an intensification of these displacement fields and it is registered as an increase in X-ray microstrain immediately after the onset of straining even in the nominally elastic regime in the absence of dislocation activity as demonstrated in [31].

Further increase of strain leads to intergranular cracking. After 3% of tensile strain cracks nucleate at first at high-angle grain boundaries of mixed character which are oriented more or less perpendicular to the direction of applied strain. They exhibit the highest tensile stresses. This excludes relaxation mechanisms as grain boundary sliding. The cracks then propagate along adjacent grain boundaries. Quite often the crack starts to open from triple junctions. This can be understood in terms of the excess volume, which is usually higher in triple junctions than in grain

boundaries and which makes them "weaker" as grain boundaries. Additionally, of course, triple junctions display the stress concentrations from the anisotropic elastic behavior of the neighboring grains. It was not possible to distinguish between these two effects. Intergranular cracking also occurs at compressive deformation beyond 5% of total strain. However, these cracks are relative small. They are nucleated at grain boundaries oriented parallel to the direction of applied strain and remain localized within these grain boundaries. Extension of these cracks into neighboring grain boundaries was never observed in compressive loading. This is most probably due to the general loading characteristic which exerts sufficiently high tensile strains perpendicular to the direction of compressive loading only to grain boundaries which are more or less ideally oriented, while all other grain boundaries see high shear and compressive strains. In contrast, tensile loading leads to opening stresses on most of the boundaries.

Similar brittle behavior of nanocrystalline palladium specimens with average grain sizes of 10 and 65 nm was found experimentally in tensile tests [32]. Although fracturing also appears unavoidable in tensile experiments, the cracking may be of different origin in the experiments since the ease of fracture in the simulations presented here is linked to the unrealistically low surface energy.

Increasing the compressive strain all types of dislocation activity – partial dislocations, twinning and full dislocations – are involved in the deformation process. It is interesting to note, that twinning begins earlier than the activity of full dislocations. However, an analysis of the generalized planar fault energy curves for stacking and twin fault planar defects for the von Sydow potential shows that twinning is expected to be observed later than the formation of full dislocations. The reason, as also mentioned in [9], the local stress intensity in the grain boundaries. After the emission of the leading partial the stress state in the boundary at the location of the emission of the first partial is relieved while the local stresses in adjacent positions are increased. Consequently the emission of a second partial dislocation at a neighboring site is strongly favored. This leads to a somewhat increased propensity of nanocrystalline metals to twinning as compared with the deformation by dislocations.

Figure 12 displays the fragment of the stress-strain curve for uniaxial compression at a strain rate of $10^8\ s^{-1}$. The circle on the curve denotes the moment when the first extended partial dislocation was observed in our simulations. Comparison with a typical macroscopic yield criterion as, 0.2% of plastic strain, does not agree well. Dislocation emission occurs at 0.7% of plastic strain. A criterion, proposed in [33], suggesting that the change from micro- to macroplasticity occurs at a third of the elastic modulus E gives a much better agreement with the results of our simulations.

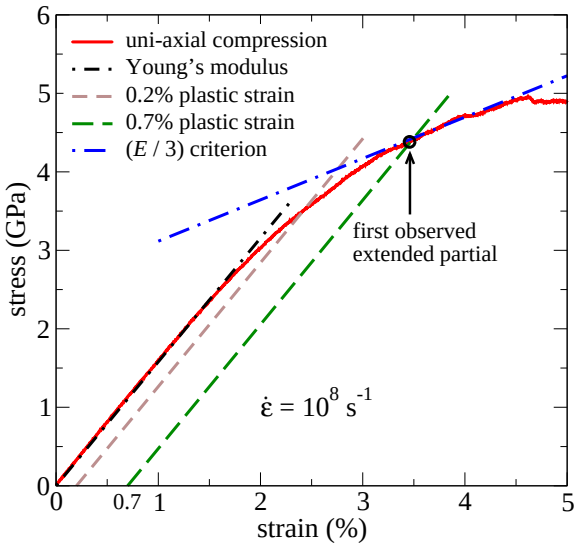

Figure 12: Stress-strain curve at an applied uniaxial compressive strain. A comparison between different definitions of elasto-plastic transition is shown.

6 Conclusions

Nanocrystalline palladium at room temperature exhibits different deformation mechanisms during uniaxial tensile and compressive straining.

1. Nanocrystalline palladium described with the potential used here responds to the tensile straining by fracturing. Cracks start to open from triple junctions and then propagate along the high-angle grain boundaries oriented perpendicular to the direction of applied strain. Locations of cracking are independent of applied strain rate.

2. No extended partial or full dislocations are observed during tensile deformation. Several partial and full dislocation embryos exist near grain boundaries on the slip planes with no necessarily highest Schmid factor. These embryos are strongly pinned by grain boundaries.

3. Strong inhomogeneous localized bending inside the grains is found to be an important deformation mechanism in addition to grain boundary accommodation processes.

4. Extended partial dislocations are observed during compressive straining. At higher strains the deformation mechanism involves full dislocations and twinning. However, their contribution to the total strain is insignificant. The main deformation mechanism is sliding in grain boundaries.

5. Further increase of straining leads to cracks nucleation at the grain boundaries parallel to the direction of applied strain. These cracks are small and localized within these grain boundaries.

Acknowledgment

Financial support by the DFG through project Gu 367/18 and through the research group FOR 714 is gratefully acknowledged. We are grateful to P.M. Derlet and H. van Swygenhoven for supplying the initial nanocrystalline model structure. Computational resources were provided by the Steinbuch Centre for Computing (SCC Karlsruhe, HLRS).

References

[1] Kumar KS, Van Swygenhoven H, Suresh S. Acta Mater 2003;51:5743.

[2] Schiøts J, Di Tolla FD, Jakobsen KW. Nature 1998;391:561.

[3] Sanders PG, Eastman JA, Weertman JR. Acta Mater 1997;45:4019.

[4] Van Swygenhoven H, Spaczer M, Caro A, Farkas D. Phys Rev B 1999;60:22.

[5] Van Swygenhoven H, Spaczer M, Caro A. Acta Mater 1999;47:3117.

[6] Derlet PM, Hasnaoui A, Van Swygenhoven H. Scripta Mater 2003;49:629.

[7] Schiøtz J, Vegge T, Di Tolla FD, Jakobsen KW. Phys Rev B 1999;60:11971.

[8] Yamakov V, Wolf D, Phillpot SR, Mukherjee AK, Gleiter H. Nature Mater 2004;3:43.

[9] Van Swygenhoven H, Derlet PM, Frøseth AG. Nature Mater 2004;3:399.

[10] Kadau K, Germann TC, Lomdahl PS, Holian BL, Kadau D, Entel P, Kreth M, Westerhoff F, Wolf DE. Metall and Mater Trans 2004;35A:2719.

[11] Van Swygenhoven H, Derlet PM, Frøseth AG. Acta Mater 2006;54:1975.

[12] Derlet PM, Gumbsch P, Hoagland R, Li J, McDowell DL, Van Swygenhoven H, Wang J. MRS Bulletin 2009;34:184.

[13] Dillamore II, Smallman RE. Phil Mag 1965;12:191.

[14] http://www.itap.physik.uni-stuttgart.de/∼imd/index.html

[15] Bitzek E, Koskinen P, Gähler F, Moseler M, Gumbsch P. Phys Rev Lett 2006;97:170201.

[16] von Sydow B, Hartford J, Wahnström G. Comput Mater Sci 1999;15:367.

[17] Hartford J, von Sydow B, Wahnström G, Lundqvist BI. Phys Rev B 1998;58:2487.

[18] Brandstetter S, Derlet PM, Van Petegem S, Van Swygenhoven H. Acta Mater 2008;56:165 .

[19] Honeycutt JD, Andersen HC. J Phys Chem 1987;91:4950.

[20] Li J, Modelling Simul Mater Sci Eng 2003;11:173.

[21] Bitzek E, Derlet PM, Anderson PM, Van Swygenhoven H. Acta Mater 2008;56:4846.

[22] Van Swygenhoven H, Derlet PM. Phys Rev B 2001;64:224105.

[23] Cheng Y, Mrovec M, Gumbsch P. Mat Sci Eng A 2008;483-484:329.

[24] Asaro RJ, Suresh S. Acta Mater 2005:53:3369.

[25] Lu L, Shen YF, Chen XH, Qian LH, Lu K. Science 2004;304:422.

[26] Zhang X, Misra A, Wang H, Nastasi M, Embury JD, Mitchell TE, Hoagland RG, Hirth JP. Appl Phys Lett 2004;84:1096.

[27] Jin ZH, Gumbsch P, Ma E, Albe K, Lu K, Hahn H, Gleiter H. Scripta Mater 2006;54:1163.

[28] Jin ZH, Gumbsch P, Albe K, Ma E, Lu K, Gleiter H, Hahn H. Acta Mater 2008;56:1126.

[29] Brandl C, Bitzek E, Derlet PM, Van Swygenhoven H. Appl Phys Lett 2007;91:111914.

[30] Stukowski A, Markmann J, Weissmüller J, Albe K. Acta Mater 2009;57:1648.

[31] Markmann J, Bachurin D, Shao L, Gumbsch P, Weissmüller J. EPL 2010;89:66002.

[32] Rösner H, Boucharat N, Markmann J, Padmanabhan KA, Wilde G. Mat Sci Eng A 2009;525:102.

[33] Thilly L, Van Petegem S, Renault PO, Lecouturier F, Vidald V, Schmitt B, Van Swygenhoven H. Acta Mater 2009;57:3157.